The 2025 World Congress on
Advances in Structural Engineering and Mechanics (ASEM25)
BEXCO, Busan, Korea, August 11-14, 2025

Surface Subsidence Detection in a Coastal City Using MT-InSAR and Sentinel-1A Data: A Case Study of Busan Station, South Korea

*Lang Fu[1)], Taeyong Park[2)], Jeongeun Kim[3)], Hyungjoon Seo[4)]

[1)] *Department of Civil and Environmental Engineering, University of Liverpool, UK L69 7ZX, UK*
[2), 3), 4)] *Department of Civil Engineering, Seoul National University of Science and Technology, Seoul 01811, Korea*

[1)] L.Fu8@liverpool.ac.uk [2)] phnty000@seoultech.ac.kr [3)] lkk109s@naver.com
[4)] hjseo@seoultech.ac.kr *(corresponding author)*

ABSTRACT

Ground subsidence can lead to significant geological hazards, resulting in substantial losses of life and property. As the largest port city and the second-largest metropolis in South Korea, as well as one of the busiest ports in the world, Busan has drawn increasing attention regarding its land subsidence issues. Investigating the characteristics of ground deformation in this area is essential for understanding the underlying changes in the urban geological environment and provides a scientific basis for urban planning and disaster mitigation. The combination of soft coastal soil and rapid urbanization in Busan increases the risk of ground subsidence. This study focuses on the Busan Station area utilizing Sentinel-1A satellite data and MT-InSAR (Multi-Temporal InSAR) techniques to monitor and analyze surface deformation from 2016 to 2025. In addition, the analysis will be integrated with the geological and infrastructural characteristics of the Busan Station area to better understand the spatial patterns and possible causes of subsidence. MT-InSAR enables millimeter-scale detection of long-term ground movement, with high spatial and temporal resolution, making it highly suitable for urban deformation monitoring. The results are expected to provide reliable data support and scientific insights for subsidence monitoring, risk assessment, and sustainable urban development in Busan and other coastal cities.

Key Words: Ground Subsidence; MT-InSAR; Remote Sensing

[1)] Ph. D Student
[2)] Undergraduate Student
[3)] Undergraduate Student
[4)] Associate Professor

1. INTRODUCTION

Ground subsidence is a widespread geohazard that occurs when the Earth's surface gradually or suddenly sinks due to natural or human-induced processes(Solari et al., 2016). This phenomenon can result from factors such as the compaction of unconsolidated soils, groundwater over-extraction, underground excavation, and long-term building loads (Ochoa-González et al., 2018; Ramirez et al., 2022). In urban areas, ground subsidence can have severe consequences, including damage to buildings and infrastructure, increased flooding risk, and disruption of transportation networks. With the rapid pace of global urbanization and the expansion of cities into geologically unstable areas, the need for continuous and accurate monitoring of ground deformation has become increasingly urgent. Among various urban environments, coastal cities are especially vulnerable, as they are often built on soft, water-saturated soils and undergo intensive land reclamation and infrastructure development(Liu et al., 2022). The complexity of subsidence mechanisms in these settings makes early detection and long-term analysis critical for risk management and sustainable development.

In recent years, satellite-based remote sensing technologies have demonstrated significant potential for detecting and quantifying ground deformation in urban areas. Among them, InSAR (Interferometric Synthetic Aperture Radar) stands out due to its advantages of all-weather capability, wide spatial coverage, and high measurement accuracy, effectively addressing several limitations of traditional ground-based surveying methods(Liu, 2005).Early studies, such as that by Gabriel et al., confirmed that D-InSAR (Differential InSAR) can detect surface displacements at sub-centimeter scales(Gabriel et al., 1989). However, D-InSAR is also subject to several constraints, including temporal and spatial decorrelation, atmospheric delay, and orbit inaccuracies(Hanssen, 2001; Zebker et al., 1997). As the technique has advanced from D-InSAR to Multi-Temporal InSAR (MT-InSAR), its focus has shifted from large deformation events to the detection of subtle, long-term ground movements. This transition has not only improved the accuracy to the millimeter level but also greatly reduced atmospheric noise effects. Nowadays, MT-InSAR has been widely used for ground subsidence monitoring in complex urban environments(He et al., 2025; Zhang et al., 2025).

MT-InSAR techniques generally fall into two categories: PS (Permanent Scatterer) and SBAS (Small Baseline Subset) approaches. PS-InSAR identifies stable point targets that maintain high coherence over time, typically linked to man-made structures(Ferretti et al., 2002b; Hooper et al., 2004; Hooper, 2006). In contrast, SBAS uses interferograms with short baselines and extracts deformation by averaging the signals of spatially coherent scatterers over short temporal intervals(Berardino et al., 2003). However, in low-coherence areas such as vegetation, bare soil, or reclaimed land, PS points are often sparse. In such cases, DS offer a useful complement by capturing deformation from statistically homogeneous surfaces(Even & Schulz, 2018). In this study, PS and DS

points are jointly used to increase the spatial density of measurement points, which improves the continuity and coverage of the subsidence map, especially in urban environments. This integrated approach is particularly beneficial for coastal urban areas like Busan, where a mix of dense infrastructure and reclaimed land creates challenges for single-method deformation analysis.

Despite the growing maturity of MT-InSAR techniques, several technical and practical limitations remain in their application to urban deformation monitoring. In particular, the effective extraction of coherent targets in spatially heterogeneous environments continues to be a challenge. Urban areas often exhibit a mix of high-rise infrastructure, open spaces, and decorrelated areas, where relying solely on PS or DS points may lead to sparse or discontinuous deformation maps. Although the integration of PS and DS observations has been proposed to overcome this issue, its performance in short-term monitoring scenarios is still not fully understood. This study aims to evaluate the effectiveness of PS-DS integration using a one-year Sentinel-1A dataset in a densely built coastal city. The objective is to enhance measurement point density and spatial completeness, and to assess the feasibility of capturing localized deformation over short time scales with high spatial detail.

2. STUDY AREA AND DATA

2.1 Study Area

The study area is in the Dong-gu District of Busan, South Korea, a coastal metropolitan city situated in the southeastern part of the Korean Peninsula. Busan is the country's second-largest city and a critical hub for transportation, logistics, and commerce. The area of interest centers around Busan Station, a major intermodal transportation node that connects intercity rail, subway, and regional transit systems. The surrounding area is characterized by a dense concentration of built-up infrastructure, including high-rise residential buildings, commercial centers, and road networks.
Topographically, the Busan Station area is relatively flat, with slight elevation gradients from the inland to the coastal margin. The subsurface is primarily composed of unconsolidated sediments, such as silts and clays, which are generally compressible and prone to long-term settlement under sustained loading(Park et al., 2020). The combined effect of high urban surface load and compressible soil layers make the area susceptible to subtle ground deformation. The spatial extent of the study area is shown in Figure 1. The red circle highlights the Busan Station area in Dong-gu District, which serves as a major transportation and commercial hub.

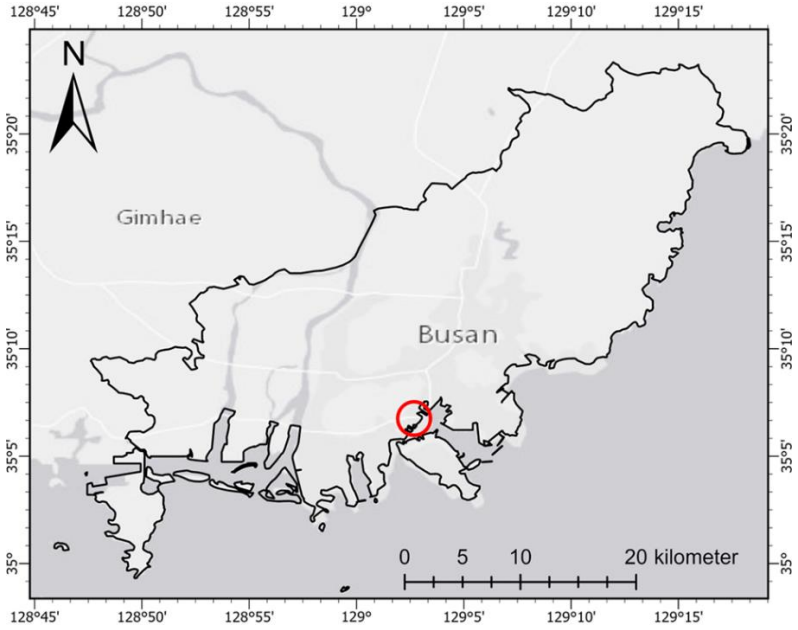

Fig. 1 Geographic location of the study area in Busan

2.2 Dataset

A total of 30 Sentinel-1A SAR images were used in this study, acquired between 14 March 2024 and 21 March 2025. All data were collected in descending orbit using the IW (interferometric wide swath) mode. The images have VV (vertical–vertical) polarization and a 12-day revisit interval and are provided as SLC (single look complex) products by the ESA (European Space Agency). This acquisition frequency ensures sufficient temporal density for time-series deformation retrieval within a one-year observation window.

Topographic phase removal was carried out using a DEM (digital elevation model) from the SRTM (Shuttle Radar Topography Mission) with a spatial resolution of 30 meters. Precise orbit ephemerides were obtained from the Copernicus POD (Precise Orbit Determination) service to correct satellite geometry and improve co-registration accuracy. Preprocessing steps included image co-registration, interferogram generation, coherence estimation, and network optimization. The resulting interferometric stack was used as input for multi-temporal InSAR analysis based on a combination of permanent and distributed scatterers.

3. METHODOLOGY

To effectively address the problem of spatio-temporal decorrelation, this study integrates two complementary multi-temporal InSAR techniques: SBAS-InSAR and PS-InSAR. While SBAS is well-suited for capturing distributed deformation in low-coherence areas, PS-InSAR enables high-precision monitoring over temporally stable scatterers. The following sections present the fundamental principles of both approaches.

3.1 SBAS-InSAR

The SBAS-InSAR technique, originally proposed by Berardino is a multi-temporal InSAR approach designed to estimate ground deformation by generating multiple interferograms with short temporal and spatial baselines(Berardino et al., 2003). By reducing decorrelation and atmospheric noise effects through baseline constraints and temporal averaging, SBAS-InSAR enables reliable phase measurements in DS areas, such as vegetated, agricultural, or bare-soil surfaces.

If $N+1$ SAR images are acquired from t_0 to t_N, the images are divided into Z short baseline subsets for the spatio-temporal baseline constraints. In each subset, the images are paired according to the short baseline criterion, and the interferograms are generated after differential interference processing. If N is specified to be an odd number, a total of M differential interferograms are generated from Z sets of images, and M can be expressed as:

$$\frac{N+1}{2} \leq M \leq N \times \frac{N+1}{2} \tag{1}$$

where N is the number of SAR images and M is the number of differential interferograms.

Taking t_0 as the initial moment, the cumulative shape variable $d(t_i, x, r)\ t \in (i = 1, \ldots \ldots, N)$ of a certain image element (x, r) in the line-of-sight direction at t with respect to the moment of to is the quantity to be solved. If 2 SAR images at t_b and t_a (t_a is earlier than t_b) are paired to generate the k[th] differential interferogram, the resulting phase is $\eta\xi(t_k, x, r)\ k \in (i = 1, \ldots \ldots, M)$. Neglecting the phase error due to noise such as atmospheric effects and elevation residuals, the phase at (x, r) is

$$\eta(t_k, x, r) = \eta\xi(t_b, x, r) - \eta\xi(t_a, x, r) = \frac{4\pi[d(t_b, x, r) - d(t_a, x, r)]}{\lambda} \tag{2}$$

where $\eta\xi(t_a, x, r)$ is the image phase at moment t_a ; $\eta\xi(t_b, x, r)$is the image phase at moment t_b; $d(t_a, x, r)$is the line of sight oriented morphology at moment t_a; $d(t_b, x, r)$ is the line of sight oriented morphology at moment t_b.

In actual processing, in addition to including the phase changes caused by the surface deformation, the error terms such as atmospheric delay, orbit error, elevation residuals and other noises are also inevitably superimposed. For this reason, the differential interferometric phase needs to be further modeled as an error and separated and corrected in the deformation extraction process. By establishing time-series observation equations for multiple short-baseline differential interferograms and employing inversion techniques such as the SVD method, surface deformation information can be extracted on a continuous time series while suppressing the effect of errors.

3.2 PS- InSAR

The PS-InSAR technique, initially introduced by Ferretti et al., utilizes a stack of co-registered SAR images acquired over the same area to detect long-term ground deformation(Ferretti et al., 2002b). A single master image is selected to minimize spatial

and temporal baselines across the stack, thereby ensuring high coherence among all interferometric pairs. The master is typically chosen near the center of the temporal and spatial baseline distribution.

Using this configuration, a series of SLC images is co-registered with respect to the master image, producing N interferograms from N+1 SAR acquisitions. After removing the topographic phase component using DEM, the residual interferometric phase at a given pixel location is influenced by several factors, including surface deformation, DEM error, orbital inaccuracies, atmospheric delay, and spatio-temporal decorrelation. The phase of the kth interferogram can be modeled as follows (Ferretti et al., 2002a):

$$\phi^k = \frac{4\pi}{\lambda} \times \frac{B_\perp^k}{R \sin\theta} h + \frac{4\pi}{\lambda} T^k v + \phi_{atm}^k + \phi_{orb}^k + \phi_{noise}^k \quad (3)$$

In this equation, the first term represents the phase contribution due to DEM error (h), where $B_\perp^k$ is the perpendicular baseline, R is the slant range, and θ is the incidence angle. The second term accounts for the linear motion of the scatterer, where T^k is the temporal baseline vector and v is the deformation rate. ϕ_{atm}^k denotes the atmospheric phase delay caused by spatiotemporal variations in water vapor. ϕ_{orb}^k represents residual orbital errors due to inaccuracies in satellite orbit data, and ϕ_{noise}^k accounts for temporal and geometrical decorrelation noise. These decorrelation effects typically arise from changes in the target's scattering characteristics, particularly over vegetation or non-urban surfaces.

3.3 MT- InSAR Processing

The initial preprocessing of Sentinel-1A SAR data was performed using the ISCE (Interferometric Synthetic Aperture Radar Scientific Computing Environment)(Fattahi et al., 2016; Yunjun et al., 2019). This stage included precise co-registration of SLC images, baseline calculation, and generation of interferometric pairs based on a temporal–spatial baseline threshold. Only interferograms with high coherence potential and minimal perpendicular baseline length were retained for further analysis. All generated interferograms and their associated metadata were subsequently converted into a StaMPS-compatible format for multi-temporal InSAR analysis.

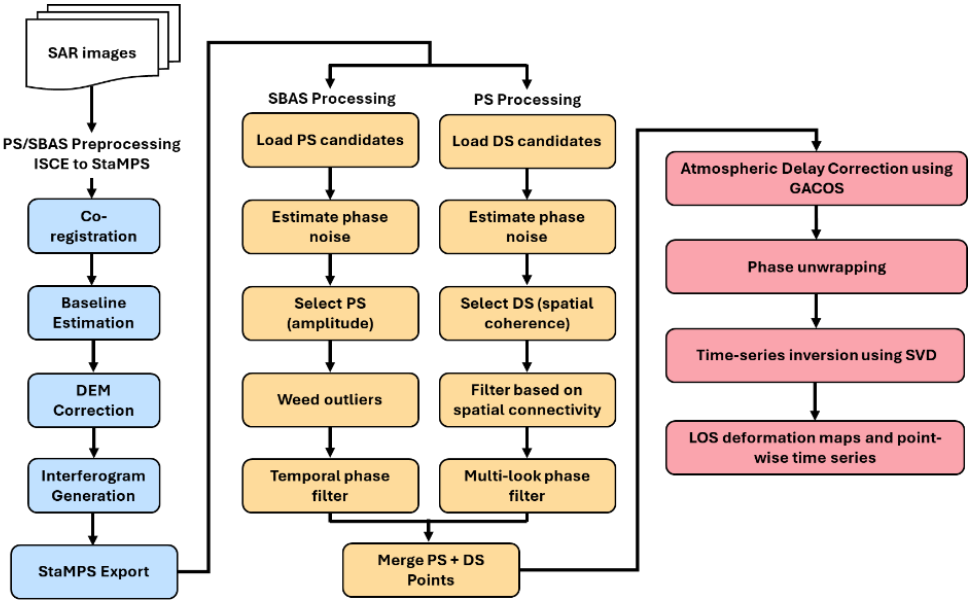

Fig. 2 Workflow

As shown in figure 2, the subsequent processing steps were carried out using StaMPS, including the extraction of PS and DS. These two branches follow different strategies for selecting coherent targets and were both applied in this study to improve spatial coverage and measurement reliability.

4. RESULTS

The average deformation rate of Busan was calculated using MT-InSAR, as shown in figure 3. In this study, the LOS (line-of-sight) direction deformation is used to analyze its spatial and temporal characteristics. Positive values indicate motion close to the satellite (uplift) and negative values indicate motion away from the satellite (subsidence).

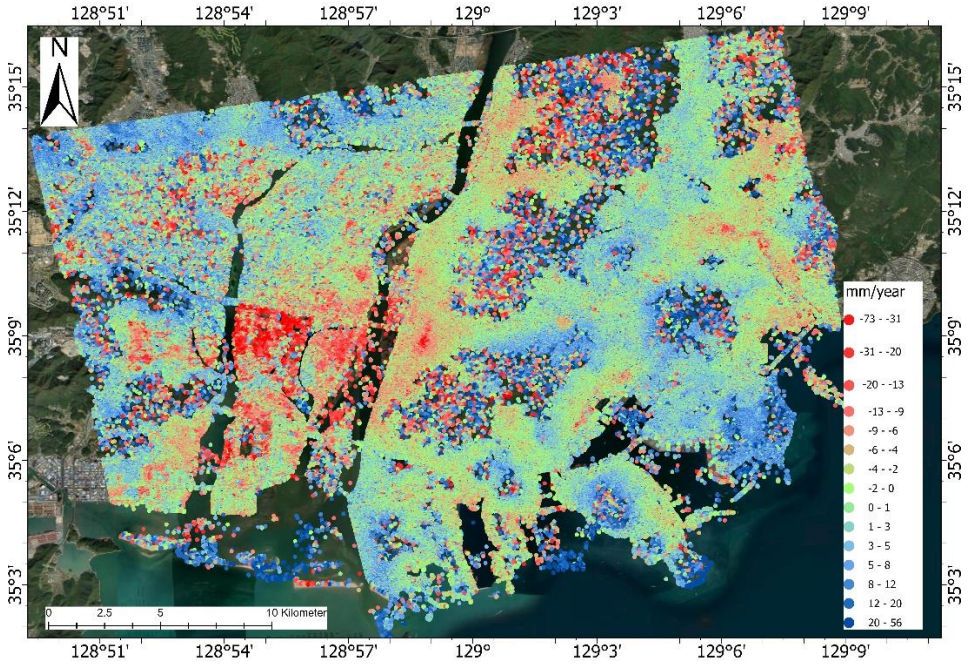

Fig. 3 Spatial Distribution of Annual LOS Deformation in the Southern Coastal Area

The LOS deformation velocity exhibits significant spatial heterogeneity across the study area. Inland areas remain largely stable, with deformation rates predominantly ranging from −15 mm/year to +5 mm/year. In contrast, more pronounced subsidence is observed in the southwestern and southeastern coastal areas, where localized deformation exceeds −30 mm/year. The maximum recorded subsidence rate is approximately −73 mm/year. This spatially uneven deformation pattern indicates that areas along the coast, especially those experiencing intensive urban development or located near river mouths, are more susceptible to ground instability.

To further investigate localized subsidence patterns, a focused analysis was conducted on the Busan Station area, which is situated near the central urban area and coastal transportation corridor. Figure 4 presents the LOS deformation velocity field around Busan Station.

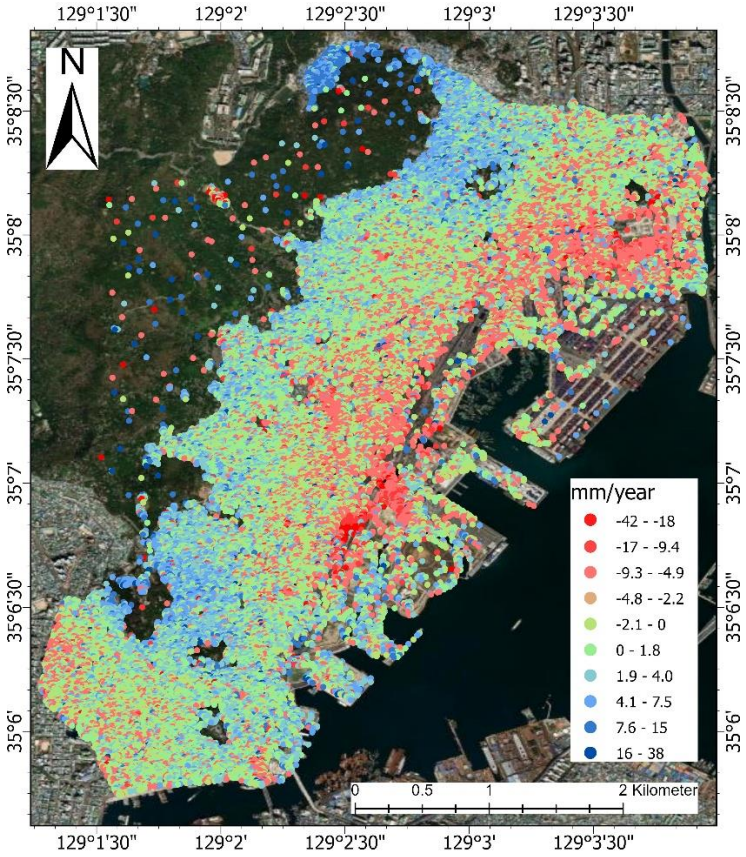

Fig. 4 Busan Station Surrounding LOS Rate Results

The area exhibits a concentrated area of subsidence centered around major transport infrastructure and coastal development sites. Most deformation rates in this area range between −10 mm/year and 0 mm/year, with several hotspots exceeding −20 mm/year. The maximum observed subsidence reaches approximately −42 mm/year. These high-deformation clusters are primarily located near the harbor area, station square, and adjacent commercial blocks. In contrast, the northern part of the frame shows relatively stable conditions, with minor uplift observed in isolated areas. The deformation pattern suggests that localized ground instability may be related to land use intensity, reclaimed land foundations, or underground structural activity.

To investigate the temporal characteristics of localized deformation within the Busan Station area, 5 monitoring points (Area 1 to Area 5) were selected based on their spatial context, structural function, and proximity to potential disturbance sources. Area 1 and Area 2 are situated near active construction sites, where field observations indicated the onset of measurable deformation beginning in February 2025. Area 3 and Area 4 are located within the central railway zone and along the road–rail interface, respectively, allowing analysis of subsidence patterns related to transportation infrastructure. Area 5 is positioned on the rooftop structure of the Busan Station building, which is supported by vertical columns. This point was chosen to assess the stability of

the upper station structure. The spatial distribution of these points is shown in Figure 5, serving as a reference for the subsequent time-series analysis.

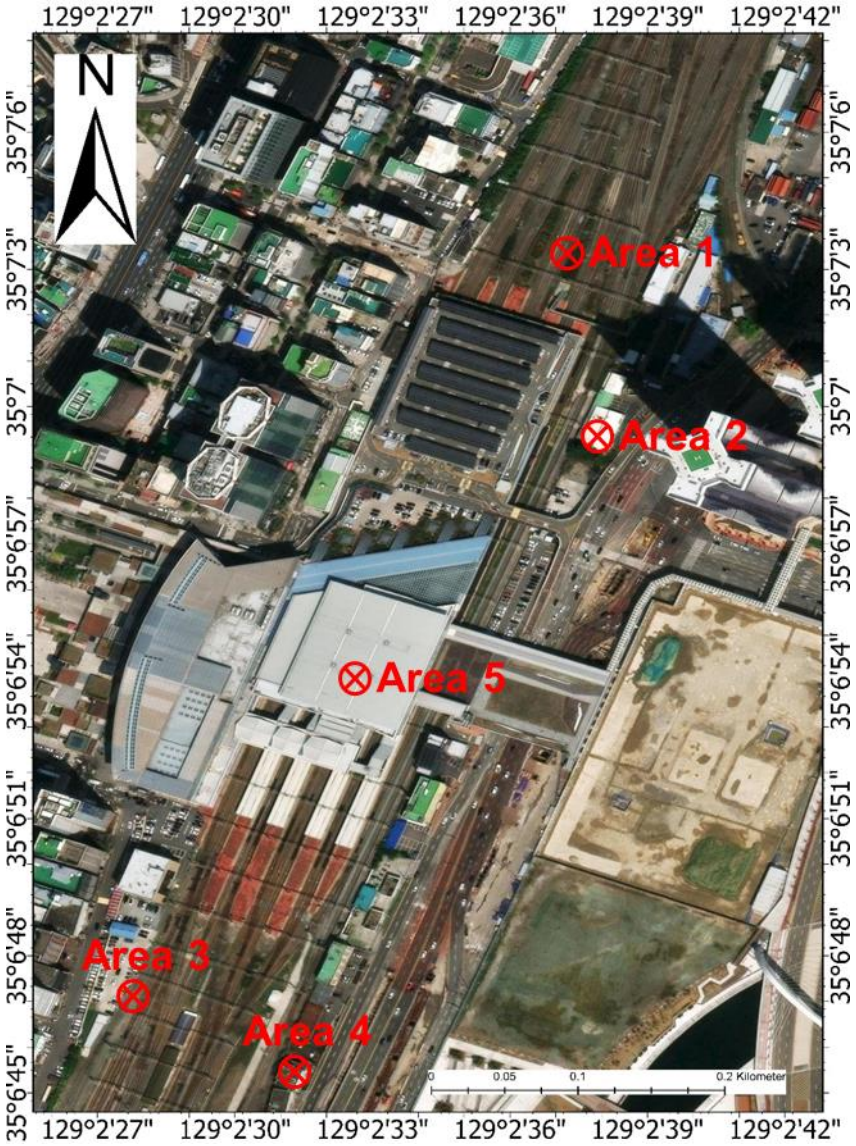

Fig. 5 Deformation Position Selection

The spatial distribution of the selected points reflects their structural and locational context, but their temporal deformation characteristics require further examination. Figure 6 presents the cumulative LOS displacement time series for the five points, allowing for comparative analysis of their deformation behavior over time.

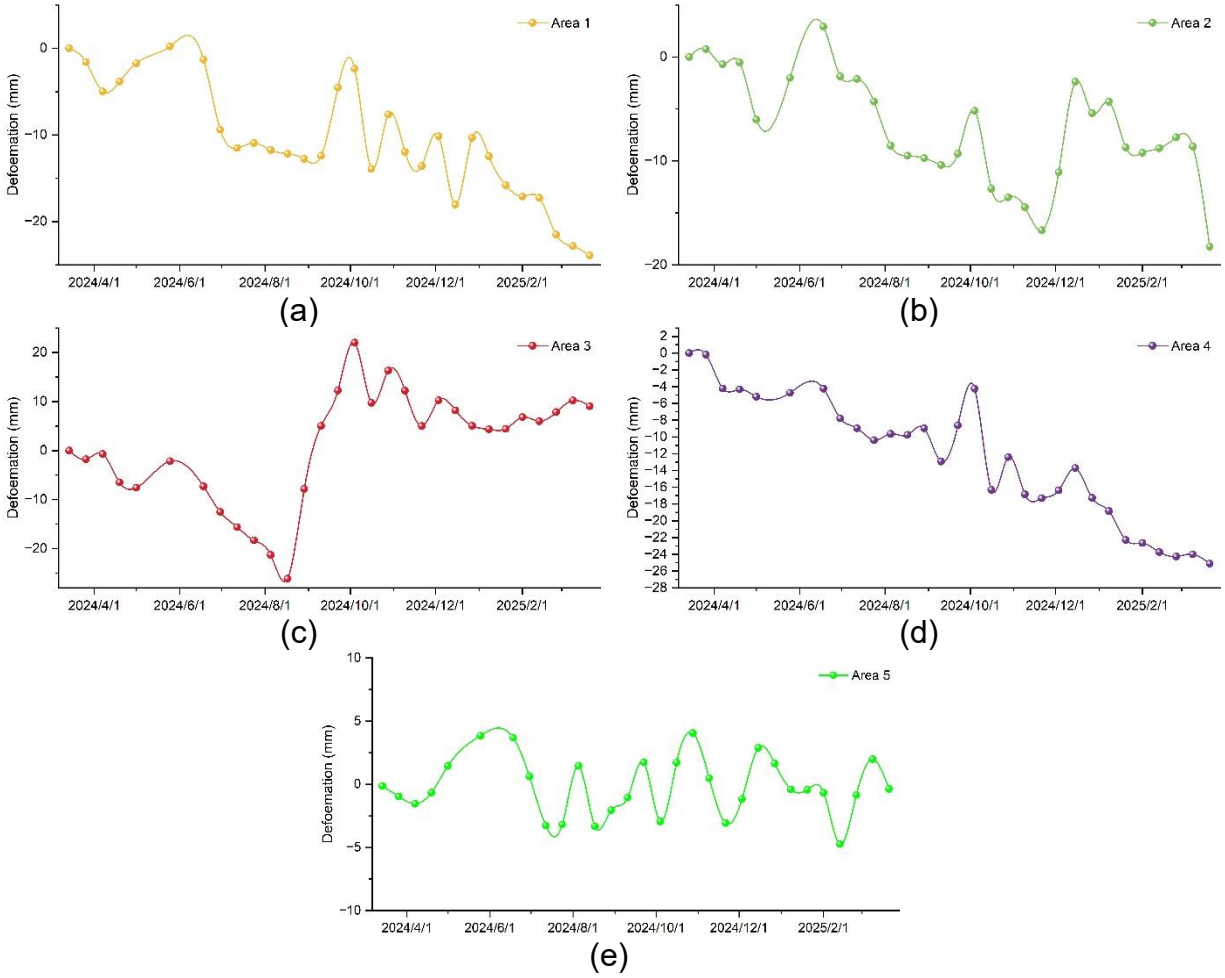

Fig. 6 Deformation time-series data from Area1 to Area5

The five monitoring points within the Busan Station area exhibit diverse temporal deformation behaviors. Area 1 and Area 2, both located near ongoing construction zones, show a sustained downward trend, with cumulative LOS displacements of approximately −24 mm and −19 mm, respectively. Field investigation suggests that ground subsidence in these areas began to intensify after February 2025, likely due to construction-induced changes in subsurface stress conditions.

In contrast, Area 3 presents a distinct non-linear deformation pattern. It experienced continuous subsidence before August 2024, reaching a maximum of −26 mm, followed by a sharp reversal and gradual uplift, eventually recovering to approximately +10 mm by early 2025. Area 4, positioned at the structural transition between the railway and adjacent road infrastructure, showed the most severe and persistent subsidence, with a total displacement of −26.5 mm, indicating a stable but pronounced downward trend.

Area 5, located on the rooftop structure of the station building, differs from the other points by exhibiting no consistent long-term trend. Instead, it displays a clear cyclical

fluctuation throughout the observation period. This oscillatory behavior may be associated with external environmental factors such as temperature variation. Overall, the five points reveal distinct deformation patterns that reflect the complex interaction of structural setting, anthropogenic activity, and environmental variability.

5. DISCUSSION

The deformation characteristics observed across the five monitoring areas in the Busan Station region reflect the combined influence of structural setting, anthropogenic activities, and localized subsurface responses. The most significant and sustained subsidence occurred in Area 4, where cumulative LOS displacement reached approximately −26.5 mm. This location lies along the structural transition between the railway and adjacent road infrastructure, a zone that may be subjected to complex stress redistribution and long-term settlement. Area 1 and Area 2, both adjacent to active construction sites, also exhibited continuous downward trends, with displacements reaching approximately −24 mm and −19 mm, respectively. Field investigations indicated that noticeable surface deformation began after February 2025, which coincides with ongoing construction activity. These trends suggest that construction-induced disturbance and subsurface consolidation likely contributed to the observed deformation.

In contrast, Area 3 demonstrated a non-linear deformation trajectory. After a prolonged period of subsidence, reaching a maximum displacement of −26 mm by August 2024, the deformation reversed and gradually shifted into an uplift phase. By early 2025, the displacement had recovered to approximately +10 mm. This reversal pattern may reflect localized soil rebound, structural unloading, or changes in subsurface water conditions. Area 5, located on the rooftop structure of the station building, displayed regular oscillatory behavior throughout the observation period, without any sustained long-term trend. The cyclic behavior observed at this location may be related to environmental variations or internal structural dynamics, although this requires further investigation.

The diversity of temporal behaviors across these monitoring areas highlights the spatial complexity of ground deformation in an urban environment. While MT-InSAR provides high-resolution deformation measurements, several uncertainties must be considered. These include atmospheric noise, phase unwrapping errors, and temporal decorrelation, particularly in non-rigid or disturbed surfaces. For example, Area 2 showed intermittent upward fluctuations during the overall subsidence trend. Such short-term variations may be attributed to temporary surface activities. These localized anomalies emphasize the importance of interpreting time-series deformation data in conjunction with structural context and site-specific knowledge.

Despite these limitations, the combined use of PS and DS targets in this study significantly enhanced spatial coverage and deformation detection reliability. This approach enabled the identification of localized instability zones and revealed subtle deformation transitions across structurally distinct environments. The findings suggest that railway corridors, structural transition zones, and construction-affected areas are

more susceptible to cumulative ground deformation and should therefore be prioritized in long-term monitoring and maintenance efforts.

Despite the robustness of the MT-InSAR approach and the clarity of the observed deformation patterns, several limitations remain in the current analysis. First, the study covers a relatively short observation period of one year, which may not fully capture long-term trends or seasonal deformation cycles. Second, while the use of five monitoring points provides localized insight, it may not comprehensively represent the deformation behavior across the entire station area. Third, the absence of in-situ validation data, such as leveling or GNSS measurements, restricts the ability to cross-verify satellite-derived displacements. Additionally, the interpretation of deformation mechanisms remains partly inferential due to the lack of auxiliary datasets, such as underground structural maps, soil profiles, or continuous meteorological records. Addressing these limitations in future work could enhance the accuracy, interpretability, and generalizability of MT-InSAR based urban deformation assessments.

6. CONCLUSION

This study employed MT-InSAR techniques to detect and analyze ground deformation in the Busan Station area using Sentinel-1A SAR data acquired between March 2024 and March 2025. A total of 30 descending-pass images were processed through a combination of PS- and SBAS-InSAR approaches, enabling millimeter-level deformation monitoring with high spatial resolution. Five monitoring points (Area 1 to Area 5) were selected for detailed time-series analysis to investigate localized deformation characteristics under various structural and environmental conditions.

The results revealed significant spatial heterogeneity in deformation behavior. Sustained and pronounced subsidence was observed in Area 4, located at a structural transition zone, with a cumulative LOS displacement of approximately −26.5 mm. Area 1 and Area 2, both adjacent to active construction zones, also exhibited continuous settlement trends, likely associated with human-induced ground disturbance. In contrast, Area 3 showed a non-linear deformation pattern, including an initial subsidence phase followed by a gradual uplift. Area 5, positioned on the rooftop structure of the station building, displayed a regular oscillatory pattern but no long-term displacement trend. These spatial and temporal variations reflect the complex interaction among infrastructure loads, ground conditions, and surface activities.

In addition to its application in the Busan Station case, the MT-InSAR approach demonstrated in this study is adaptable to other urban settings where conventional monitoring is limited by cost, accessibility, or spatial coverage. Its ability to extract high-density, temporally continuous deformation information without requiring ground-based instrumentation makes it particularly suitable for infrastructure surveillance in complex-built environments. Future research may benefit from integrating multi-source geospatial datasets, such as temperature records, underground utility maps, or construction schedules, to further interpret deformation mechanisms and improve predictive accuracy.

Acknowledgements

This work was supported by the National Research Foundation of Korea (NRF) grant funded by the Korea government (MSIT) (No. RS-2021-NR060085).

REFERENCE

Berardino, P., Fornaro, G., Lanari, R., & Sansosti, E. (2003). A new algorithm for surface deformation monitoring based on small baseline differential SAR interferograms. *IEEE Transactions on geoscience and remote sensing*, *40*(11), 2375-2383.

Even, M., & Schulz, K. (2018). InSAR deformation analysis with distributed scatterers: A review complemented by new advances. *Remote Sensing*, *10*(5), 744.

Fattahi, H., Agram, P., & Simons, M. (2016). A network-based enhanced spectral diversity approach for TOPS time-series analysis. *IEEE Transactions on geoscience and remote sensing*, *55*(2), 777-786.

Ferretti, A., Prati, C., & Rocca, F. (2002a). Nonlinear subsidence rate estimation using permanent scatterers in differential SAR interferometry. *IEEE Transactions on geoscience and remote sensing*, *38*(5), 2202-2212.

Ferretti, A., Prati, C., & Rocca, F. (2002b). Permanent scatterers in SAR interferometry. *IEEE Transactions on geoscience and remote sensing*, *39*(1), 8-20.

Gabriel, A. K., Goldstein, R. M., & Zebker, H. A. (1989). Mapping small elevation changes over large areas: Differential radar interferometry. *Journal of Geophysical Research: Solid Earth*, *94*(B7), 9183-9191.

Hanssen, R. F. (2001). *Radar interferometry: data interpretation and error analysis* (Vol. 2). Springer Science & Business Media.

He, Q., Liu, H., Wei, L., & Zhang, Z. (2025). Analysis of the Driving Factors for Land Subsidence in the Northern Anhui Plain: A Case Study of Bozhou City. *Water*, *17*(13), 1854.

Hooper, A., Zebker, H., Segall, P., & Kampes, B. (2004). A new method for measuring deformation on volcanoes and other natural terrains using InSAR persistent scatterers. *Geophysical research letters*, *31*(23).

Hooper, A. J. (2006). *Persistent scatter radar interferometry for crustal deformation studies and modeling of volcanic deformation*. Stanford University.

Liu, G. (2005). Application examples of InSAR and its limitation analysis. *Surveying and Mapping of Sichuan*, *28*(3), 139-143.

Liu, W., Zhu, J., Zhang, H., Ma, X., & Xie, J. (2022). Geological conditions of saturated soft loess stratum and influence of tunnel excavation and dewatering system on its groundwater environment. *Bulletin of Engineering Geology and the Environment*, *81*(3), 128.

Ochoa-González, G., Carreón-Freyre, D., Franceschini, A., Cerca, M., & Teatini, P. (2018). Overexploitation of groundwater resources in the faulted basin of Querétaro, Mexico: A 3D deformation and stress analysis. *Engineering Geology*, *245*, 192-206.

Park, J.-Y., Lee, S.-R., Oh, S., Lee, J. H., Jeon, J.-S., Song, Y.-S., & Park, H.-S. (2020). Critical continuous rainfall map for forecasting shallow landslide initiations in Busan, Korea. *Water*, *12*(9), 2404.

Ramirez, R. A., Lee, G.-J., Choi, S.-K., Kwon, T.-H., Kim, Y.-C., Ryu, H.-H., Kim, S., Bae, B., & Hyun, C. (2022). Monitoring of construction-induced urban ground deformations using Sentinel-1 PS-InSAR: The case study of tunneling in Dangjin, Korea. *International Journal of Applied Earth Observation and Geoinformation*, *108*, 102721.

Solari, L., Ciampalini, A., Raspini, F., Bianchini, S., & Moretti, S. (2016). PSInSAR analysis in the Pisa urban area (Italy): A case study of subsidence related to stratigraphical factors and urbanization. *Remote Sensing*, *8*(2), 120.

Yunjun, Z., Fattahi, H., & Amelung, F. (2019). Small baseline InSAR time series analysis: Unwrapping error correction and noise reduction. *Computers & Geosciences*, *133*, 104331.

Zebker, H. A., Rosen, P. A., & Hensley, S. (1997). Atmospheric effects in interferometric synthetic aperture radar surface deformation and topographic maps. *Journal of Geophysical Research: Solid Earth*, *102*(B4), 7547-7563.

Zhang, M., Pan, J., Ma, P., & Lin, H. (2025). Identification and Analysis on Surface Deformation in the Urban Area of Nanchang Based on PS-InSAR Method. *Remote Sensing*, *17*(1), 157.